Density Functional Calculations on Class III Ribonucleotide Reductase: Substrate Reaction Mechanism with Two Formates

Kyung-Bin Cho,[§] Vladimir Pelmenschikov,[#] Astrid Gräslund,[§] and Per E. M. Siegbahn*,[#]

Department of Biochemistry and Biophysics, and Department of Physics, Stockholm University, SE-106 91 Stockholm, Sweden

Received: May 9, 2003; In Final Form: October 20, 2003

The substrate reaction mechanism for class III anaerobic ribonucleotide reductase has been studied by density functional theory on a charged system involving two formates. Previous studies on small charge-neutral models yielded a rate-limiting barrier of 19.9 kcal/mol, compared to the experimental value of approximately 17 kcal/mol. The current study involves a larger model with four amino acid residues (Cys290, Asn78, Cys79, and Asn311) present in the active site, in addition to the two formates and the substrate model. All steps starting from the Cys290 radical have been considered here in contrast to only the rate-limiting part considered before. The rate-limiting step is again found to be the oxidation of formate to carbon dioxide. The highest barrier is now calculated to be as low as 11.7 kcal/mol, suggesting that a step outside of the substrate reactions is rate limiting. The model used for the substrate is a simple ribonucleotide ring, but preliminary results using the full substrate model (with a guanine base and a triphosphate chain) are also reported. These calculations show an overall agreement with the smaller substrate model calculations. The reaction mechanism presented here is highly consistent with existing experimental information.

Introduction

The family of ribonucleotide reductases (RNR) catalyzes the reduction of ribonucleotides to deoxyribonucleotides (Scheme 1), required for DNA synthesis. This seemingly simple substitution of 2′OH with H goes through a complicated radical mechanism.[1−4] There are to date three classes of RNRs known, differing in structure, cofactor requirements, and radical generation. A crystal structure of the reductase components of a class III RNR from bacteriophage T4 has been solved.[5] The structure was compared to that of the large subunit of a class I RNR reported earlier,[6] and similar folds as those found in class I RNR were observed. The two enzymes, class I RNR and class III RNR, may have a common ancestor, and the catalytic mechanisms may share some common properties. As a background to our study on class III RNR, some relevant properties of class I RNR will be presented first.

Class I RNR is the most studied of the RNRs. This enzyme is found in mammalian cells and *E. coli* bacteria under aerobic conditions. The active enzyme consists of two homodimeric proteins, R1 and R2. Protein R2 contains a diiron center,[6] which is involved in the formation of the radical needed in the redox chemistry of the enzyme.[7−13] Protein R2 is also known to contain a tyrosyl residue (Tyr122, *E. coli* numbering) close to the diiron site, where the free radical is harbored between the substrate reactions. During each turnover, the radical character is transported back and forth to the active site in protein R1 where the substrate (ribonucleotide diphosphate, NDP) becomes reduced. This takes place over a distance of approximately 35 Å by a long range proton-coupled electron-transfer mechanism via a hydrogen-bonded chain of residues. Detailed studies of

SCHEME 1: Ribonucleotide Reduction Mediated by RNR

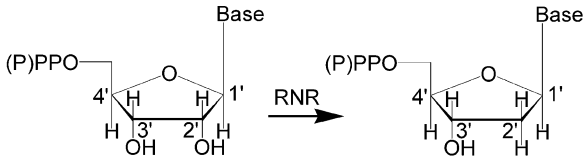

the different parts of the enzymatic reaction mechanism have been performed both experimentally and theoretically (Scheme 2).[14−20] The radical transfer chain ends at Cys439, from where the substrate reaction begins. Essential residues in the substrate site reaction in protein R1 involve Cys439, Glu441, Asn437, Cys225, and Cys462.[21,22] Following previous experimental and theoretical works,[3,14,16] Cys439 is proposed to abstract the 3′H proton, followed by hydroxyl release at the 2′-site mediated by Glu441 and Asn437, to form water. Hydrogen is then donated to 2′C from the nearby Cys225 and Cys462 complex, creating a disulfur anion bond between the cysteines.[23] The disulfur bond is later reduced by thioredoxin, glutaredoxin, and/or NrdH-redoxin systems through an electron-transfer pathway consisting of a chain of cysteines, making these systems the ultimate electron donors in the reduction mechanism. The radical character ends up at 3′C, where Cys439 returns the proton and the radical character is returned to Tyr122 in protein R2. Protein R1 also contains allosteric regulatory sites, which control the amount of the different NDPs reduced.[24] The turnover rate for class I RNR is approximately 10 s^{-1},[25] corresponding to approximately 16 kcal/mol in the rate-limiting energy barrier. A parallel study to the one presented here involving a mechanism with a negatively charged system in class I RNR has also been published recently.[26]

Like class I RNR, class III RNR is also an $\alpha_2\beta_2$ heterodimer, but it uses an iron−sulfur cluster and the cofactor *S*-adenosyl-

* Author to whom correspondence should be addressed. Phone: +46-8-55378704. Fax: +46-8-55378601. E-mail: ps@physto.se.
[§] Department of Biochemistry and Biophysics.
[#] Department of Physics.

10.1021/jp035280u CCC: $27.50
Published on Web 01/15/2004

SCHEME 2: Results of Earlier Theoretical Studies on the Substrate Reaction Mechanism of Class I RNR[14,16] and Class III RNR[38] [a]

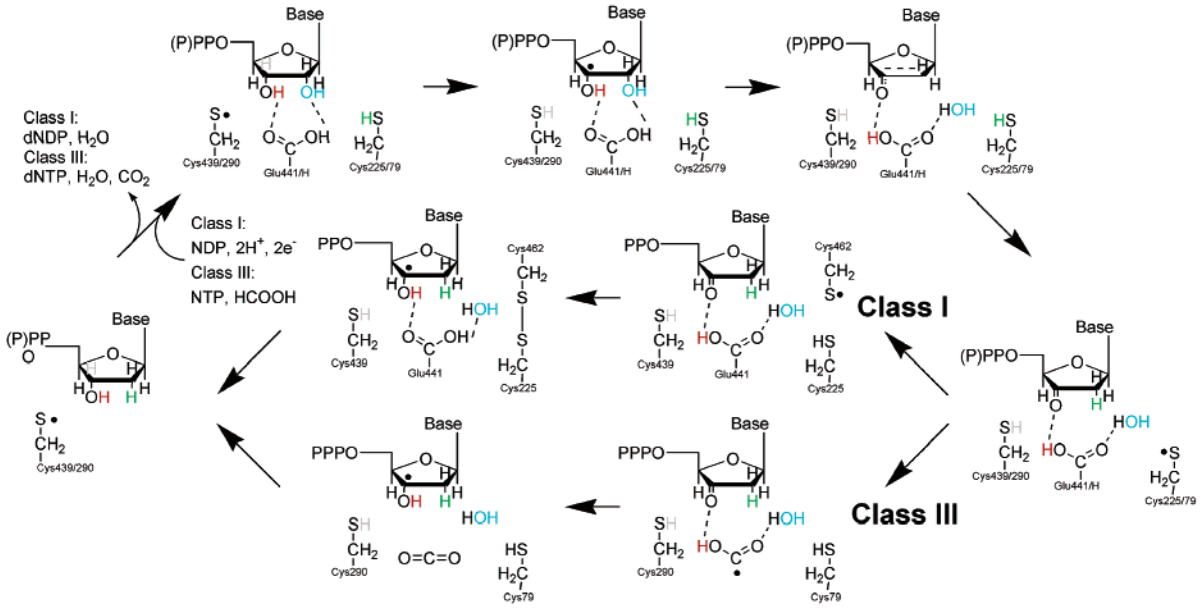

[a] Only residues essential for clarity in each step are shown.

methionine (AdoMet) to generate the radical.[27−30] AdoMet is cleaved during the reaction. The adenosyl moiety mediates transport of the radical and ultimately stores it as a glycyl radical at Gly580 (T4, *bacteriophage* numbering) in the α subunit, close to the substrate binding site. The substrate reduced is ribonucleotide triphosphate (NTP), and the enzyme is active only under strictly anaerobic conditions. Exposure to oxygen results in protein cleavage at the radical site.[30] Structural studies[5] have shown conservation of key residues involved in the class I RNR reaction mechanism: class III RNR Cys290 and Cys79, which correspond to class I RNR Cys439 and Cys225, respectively. These cysteines have indeed also been shown to be essential to the class III RNR reaction mechanism.[31,32] Cys462 is in class III RNR replaced by Asn311, and therefore, a disulfur bond cannot be formed in this case. However, an experimental study has shown that the highly conserved residues Asn311 and Asn78 instead may have important roles in the substrate reduction.[33] Site-directed mutagenesis of Asn311 to alanine resulted in 17.9% activity, whereas the mutation of Asn78 resulted in 7.6% activity. Mutation of both of these residues at the same time gave no activity at all. In addition, ^{14}C-labeling experiments have shown that formate is essential for the reaction as the ultimate electron donor, being reduced to carbon dioxide during the reaction.[34] Stoichiometric formation of deoxyribonucleotide triphosphate (dNTP) and carbon dioxide were observed in the process. The same study also mentions that when tritium-labeled formate ($^{3}HCOO^{-}$) was used, the tritium would end up in water. Comparisons have been made to pyruvate formate lyase (PFL) because of the similar three-dimensional structures, the use of glycyl radicals, and the involvement of formate in the catalytic reaction. However, the formate is a product of the PFL reaction (in contrast to class III RNR, which consumes formate and produces carbon dioxide).[35−37]

The substrate reaction mechanism of class III RNR has previously been studied theoretically in a small neutral model[38] (Scheme 2). There, formic acid was reduced to carbon dioxide through an intermediate state involving a formyl radical. The use of the neutral formic acid rather than a negatively charged formate was a necessity for the modeling, because a proton is needed to complete the reaction. The rate-limiting barrier found in this way was 19.9 kcal/mol, compared to an experimentally determined limit of about 17 kcal/mol (∼3 s^{-1}) for class III RNR. Thermal and solvent effects, as well as zero-point vibrational energies, were together found to have a large influence on the final energies (up to 9 kcal/mol) in lowering the rate-limiting barrier. The reaction mechanism obtained agreed in essence with the one proposed by Eklund and Fontecave,[39] which was obtained by structural studies and differs only in terms of the overall charge value at certain steps of the reaction. In the present study (Scheme 3), improved theoretical models have been used which include two formates, with the necessary proton attached to one of them. This makes the total charge of the model −1, in contrast to the previous neutral model. Furthermore, the model now includes Cys290, Asn78, Cys79, and Asn311 residues in all steps. NTP is modeled as a simple ribose ring. Supplementary calculations were also done with the triphosphate chain and the base (guanine) included in order to estimate possible effects on the reaction mechanism of these groups.

Computational Details

The starting structure of the enzyme was taken from the crystal structure of the class III RNR reductase from bacteriophage T4.[5] The substrate was inserted into the active site mimicking the substrate-bound crystal structure of class I RNR.[40] The residues chosen to model the active site were Asn78, Cys79, Cys290, and Asn311. The α-carbons in cysteines and *β*-carbons in asparagines were replaced by hydrogens, and these coordinates were held fixed in space during all geometry optimizations to mimic the strain of the protein backbone.

The primary model used involves the chosen amino acid residues with the substrate modeled as a simple ribose ring with no phosphate chain or base. The geometry optimizations for the ground states were done with hybrid density functional theory[41] using the B3LYP functional[42−44] as implemented in the Jaguar 4.0 program.[45] The basis set used in the geometry optimizations was lacvp, except on the sulfur and phosphorus

SCHEME 3: Total Reaction Mechanism Outlined in This Study

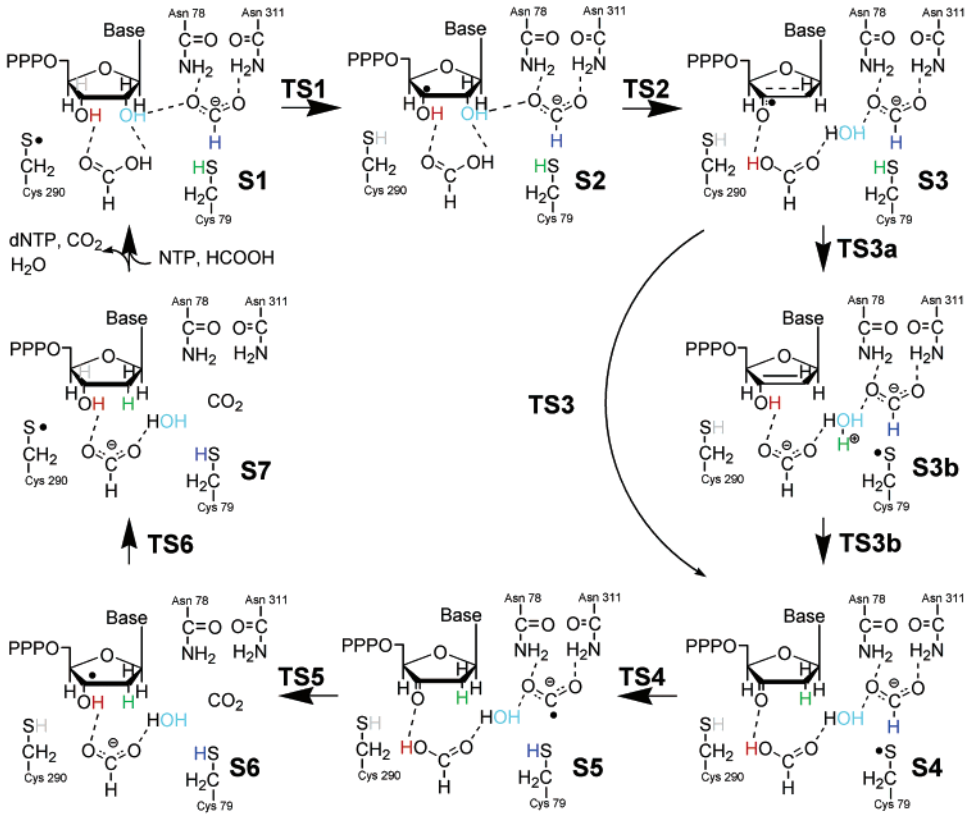

atoms where the larger lacv3p** was used. The transition state optimizations as well as all frequency calculations were done using the Gaussian 98 package,[46] using the same basis set as in the ground state optimizations. The zero-point vibrational energies were taken from these frequency calculations, although no thermal effects were included because the use of nonoptimized frozen coordinates does not give reliable entropy effects. In the previous study,[38] these effects alone were found to be small.

After a sufficiently converged geometry had been obtained, single-point large basis set (lacv3p** on all atoms) calculations were performed with Jaguar on the converged geometry to obtain accurate energies. Solvent effects were included as a dielectric medium of $\epsilon = 4$ with Jaguar and the same large basis set. The self-consistent reaction field method was used where the solvation energies were calculated iteratively using the Poisson−Boltzmann equation.

Some supplementary calculations have been done on a larger model, where a triphosphate chain has been added to the substrate model together with a guanine as a base. To keep the phosphate chain neutral, it has been triply protonated, yielding an 80-atom complex. However, the initial geometry optimizations of this large system generated unreasonably large movements of the phosphate chain. To restrain the geometry variations, an amino proton in guanine and a hydroxyl proton at the end of the phosphate chain were held fixed close to the highly conserved residues His64 and Asp67 mimicking possible hydrogen bonds to these residues. No frequency calculations were done because of the size of the system, and the zero-point vibrational energies were instead taken from the small model. The transition states in the large model were obtained by freezing one geometrical distance crucial for the transition state, the distance being taken from the smaller model calculations. Exceptions (see the results section) were the geometries for TS2 with a concerted transition state and TS5, which models an electron-transfer transition state. The former one required two distances to be frozen, and the latter one required in the end four distances and one angle to be frozen. The actual transition state energies might therefore deviate somewhat from the ones reported here. However, comparison with the smaller model showed a similar spin distribution in the larger model, which indicates that the geometries should be reasonably close to the actual transition states.

Results

The results obtained are reported and discussed in seven steps, involving eight ground states and eight transition states (named in this study S1, TS1, S2, etc.). The total charge of the system is −1, and the multiplicity is 2. The energies are summarized in Tables 1 and 2, and Scheme 3 shows the total reaction mechanism that is followed in the present study.

The starting point for our calculations is the Cys290 radical, which has been assumed to have been created by hydrogen abstraction from the nearby glycyl radical at Gly580. The inclusion of the first of the formates was made to mimic the function of Glu441 in class I RNR in facilitating the water release in the next step. The second formate was placed near the two asparagines, as there have been suggestions that the asparagines could serve as a carboxylate binding site.[5,33] The extra proton needed for the reaction was initially placed in a location that allowed it to be shared between the two formates, but in the final starting structure that was obtained, the two-formate complex was broken apart as Figure 1 shows. This structure was the lowest in energy of several alternatives and served as a good starting point for our investigations.

Step 1: Creation of the 3′C Radical (S1 → TS1 → S2). The first step involves abstraction of 3′H from the substrate by

TABLE 1: Energetics of the Small Model[a]

state	small basis set (*A*)	large basis set effect (*B*)	solvent effect (*C*)	Z_0 (*D*)	total ($A + B + C + D$)
S1	0.00	0.00	0.00	0.00	**0.00**
TS1	10.78	−3.13	+0.50	−3.63	**4.52**
S2	6.75	+0.28	+1.78	−4.04	**4.77**
TS2	8.20	−0.18	+0.76	−4.42	**4.36**
S3	6.68	−6.19	−0.20	−3.18	**−2.89**
TS3	19.67	−8.11	−1.07	−4.85	**5.63**
TS3a	7.80	−0.52	+0.01	−5.29	**2.01**
S3b	−0.91	−0.90	+3.16	−2.46	**−1.11**
TS3b	6.64	+1.94	+2.23	−4.76	**6.04**
S4	0.38	−6.25	+0.75	−0.89	**−6.00**
TS4	11.86	−10.20	−0.81	−3.53	**−2.67**
S5	11.83	−11.39	−1.10	−2.88	**−3.54**
TS5	22.05	−11.39	+1.65	−6.64	**5.67**
S6	−1.04	−15.09	+3.14	−2.47	**−15.46**
TS6	1.15	−15.00	+1.93	−3.99	**−15.92**
S7	−3.56	−13.22	+3.17	−0.33	**−13.94**

[a] All values are in kcal/mol, relative to the first column and first row.

TABLE 2: Energetics of the Large Model[a]

state	small basis set (*A*)	large basis set effect (*B*)	solvent effect (*C*)	Z_0 (*D*)[b]	total ($A + B + C + D$)
S1	0.00	0.00	0.00	0.00	**0.00**
TS1	17.45	+0.26	−3.11	−3.63	**10.97**
S2	7.40	+3.28	−2.95	−4.04	**3.69**
TS2	13.13	+2.15	−4.30	−4.42	**6.56**
S3	10.86	−2.30	−4.21	−3.18	**1.16**
TS3	28.20	−3.78	−4.51	−4.85	**15.05**
TS3a	10.84	+0.64	+0.49	−5.29	**6.68**
S3b	2.96	+4.97	−7.64	−2.46	**−2.17**
TS3b	9.10	+6.04	−3.96	−4.76	**6.42**
S4	4.53	−0.53	−5.97	−0.89	**−2.86**
TS4	17.29	−7.70	−7.08	−3.53	**−1.02**
S5	15.67	−6.98	−5.84	−2.88	**−0.03**
TS5	34.22	−11.38	−6.25	−6.64	**9.93**
S6	0.51	−14.35	+1.00	−2.47	**−15.31**
TS6	9.88	−13.16	+1.51	−3.99	**−5.76**
S7	−10.39	−9.21	+2.34	−0.33	**−17.59**

[a] All values are in kcal/mol, relative to the first column and first row. [b] Z_0 is taken from the small model, i.e., Table 1.

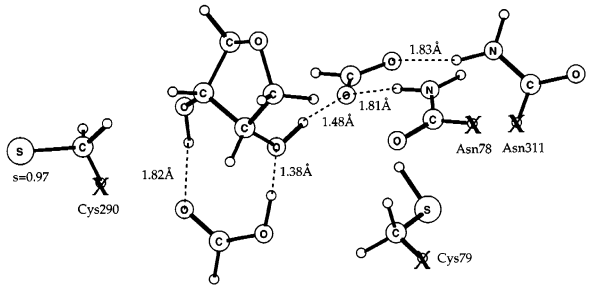

Figure 1. Optimized structure S1. Key distances and spin distributions are indicated. Atoms that are held fixed in space during geometry optimizations are marked with an X.

the Cys290 radical. The energy of the optimized transition state (Figure 2) for this step is calculated to be 4.5 kcal/mol higher than the reactant. However, this is not a true transition state, because inclusion of solvent energies makes the product state higher than the transition state. When the reaction finishes, the hydrogen initially located at the formate is now closer to the 2′OH than it is to formate and is thus well set up for the next

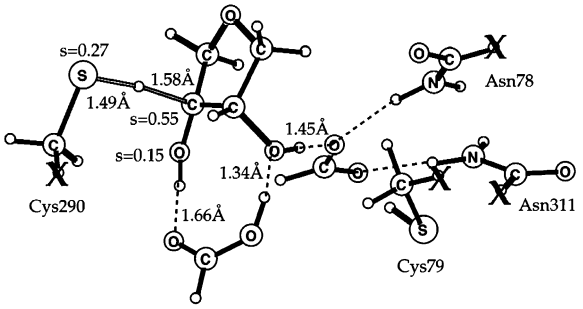

Figure 2. Transition state (TS1) for the first step.

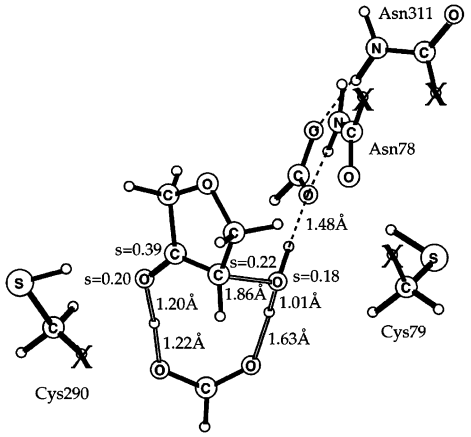

Figure 3. Transition state (TS2) for the second step.

step of water formation. The radical is now at the 3′C site. When all effects are added, the energy for the optimized product of this step is 4.8 kcal/mol (S2, Table 1).

The hydrogen abstraction from 3′C by the cysteine radical is supported by various substrate analogues and labeling experiments on class I RNR.[47−49] Similar experiments on class III RNR suggest that this step is conserved in class III RNR as well.[50,51] In addition, our parallel theoretical study on class I RNR gives similar energy values (barrier of 4.5 kcal/mol, product at 2.1 kcal/mol),[26] as expected even though the substrate site environment differs somewhat. The occurrence of this step is therefore not surprising given that consensus regarding this already existed in the field.

Step 2: Water Release and 2′C Radical Formation (S2 → TS2 → S3). This step follows the outline presented in earlier investigations.[16] The proton attached to the 3′O is transferred to the formate, at the same time as water is formed at the 2′-site. The transition state lies at 4.4 kcal/mol above S1 (Figure 3). After this step, the spin is mostly on the 2′C site (0.52). Some spin is delocalized between 3′C (0.10), 3′O (0.23), and H_2O (0.14) as well. The small but significant spin density at H_2O could be one of the reasons why the proton from Cys79 so easily attaches there in the next step. The product (S3, Table 1) is quite stable with an energy of −2.9 kcal/mol compared to S1. Because the transition state TS2 is lower in energy than S2, the calculations suggest that steps 1 and 2 may be one concerted step with the transition state close to the geometry for S2.

The concept of formate acting as a hydrogen mediator as described above was first proposed in an earlier theoretical study[16] on class I RNR, where the formate represented a model of Glu441. Because this residue is missing in class III RNR, suggestions have been made that formate would replace Glu441 in its role as an acid/base catalyst.[5,38,39] Although no direct

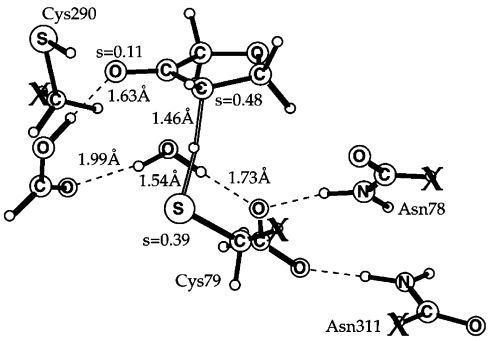

Figure 4. Transition state (TS3) for the third step.

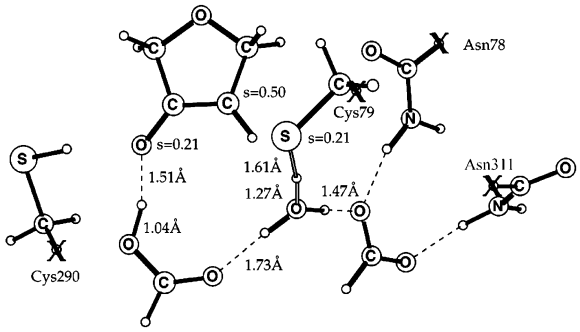

Figure 5. Transition state TS3a.

evidence exists for this assumption, quantum chemical calculations show that it is certainly possible. In yet another theoretical study, several alternatives to this step were explored.[52] In calculations on a series of small models, it was concluded that water formation requires a base, presumably a carboxylate group, at the 3′-side to abstract a proton from 3′OH. If the carboxylate group was protonated to start with as above, this reaction would indeed be the preferred one from an energetic point of view. However, if the carboxylate group is not protonated at its initial state, water formation at the 2′-site can still occur with a proton donated from a nearby donor, presumably a cysteine. For reasons described in the conclusions section, our model involves a protonated formate, and therefore, the results are in line with these observations.

Step 3: Cys79-Radical Formation (S3 → TS3 → S4). Following the scheme proposed, the radical character is now transferred to Cys79.[38,39] The next natural step is to transfer the hydrogen from Cys79 directly to the nearby 2′-carbon (Figure 4). Initially, this route was rejected, because investigations indicated that the barrier for this route would lie approximately 20 kcal/mol above S1 (calculated with the small basis set), which would be about the same barrier as for the rate-limiting step TS5. However, once the actual transition state was found, basis effects were found to be large. The transition state was at 22.6 kcal/mol (compared to S3) with a small basis set, and a subsequent large basis set calculation lowered the energy to 14.5 kcal/mol. Including zero-point energy and solvent effects, the final transition state value is at 8.5 kcal/mol.

However, in the initial set of calculations the optimizations instead led to a transfer of the cysteine proton to water, forming H_3O^+ (S3 → TS3a → S3b, Scheme 3). In addition, the substrate oxygen at the 3′-site became protonated again. Formally, this created a double bond between the 2′- and 3′-carbons, and a $HCOO^-{-}H_3O^+{-}HCOO^-$ complex was formed. After an extensive search, the transition state for this step (Figure 5) was found to lie at 2.0 kcal/mol, implying a small barrier of 4.9 kcal/mol between S3 and S3b. The product energy is −1.1 kcal/mol (S3b, Table 1). There are rather large solvent effects on the product, which is reasonable considering that there has been a considerable charge movement. The spin density is now 0.95 on the Cys79 sulfur atom.

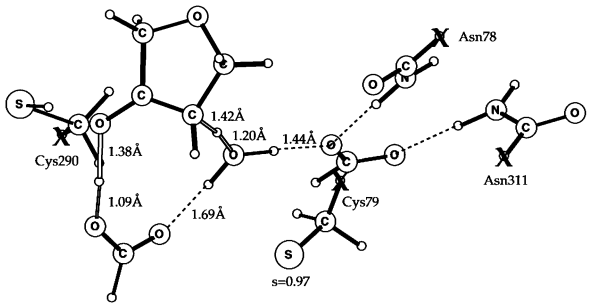

Figure 6. Transition state TS3b.

Together with TS5, the transition state TS3a was one of the more difficult ones to locate. This step involves, besides the H_3O^+ complex formation, also a proton transfer from the formate oxygen back to 3′O. In principle, one can imagine this step occurring either as a concerted process or as a two-step process where the proton transfers occur separately. Considering that TS3a has about the same distances, spin, and charge distributions on the formate and the 3′-site of the substrate as in S3, the transition state seemed likely to be the first of a two-step process. However, once the H_3O^+ complex was formed, the formate oxygen proton was found to automatically move toward 3′O. The conclusion is therefore that TS3a is a transition state for forming the H_3O^+ complex, which is immediately followed by a 3′O protonation that occurs automatically without any energy barrier.

The proton is now further transferred from the H_3O^+ complex to 2′C (S3b → TS3b → S4) over a barrier of 8.9 kcal/mol above S3 (Figure 6), which is the lowest lying state so far. No change of the spin distribution occurs, and the spin still rests on Cys79. Again in a concerted manner, the 3′O proton returns back to the formate forming a 3′-keto group at the same time as the proton is released from H_3O^+. The product is now at −6.0 kcal/mol (S4, Table 1).

The formation of the H_3O^+ complex has not been suggested before in the literature, but the optimizations straightforwardly ended up in this form. In fact, comparing TS3a with the direct protonation of 2′C (TS3), the former barrier is initially lower. One could imagine that there are some advantages with a small mobile H_3O^+ complex that can easily access the substrate and 2′C, regardless of the protein and substrate rigidity. In the class I RNR study,[26] the protonation of 2′C occurs via H_2O in a similar manner as here, making it unnecessary for Cys225 (corresponding to Cys79) to be able to reach 2′C directly and giving the whole system a certain motional flexibility. Although the degree of advantage of this motional flexibility is not clear, it should at least not be a disadvantage. Comparing barriers for the two routes, the direct route has a barrier of 8.5 kcal/mol compared to 8.9 kcal/mol for the higher one of the two steps above (TS3b). Therefore, none of the two routes can be excluded, but both routes have barriers not exceeding the rate-limiting barrier at TS5 (see below). Consequently, neither of these two routes determine the reaction rate of the catalytic reaction.

Step 4: Formyl Radical Formation (S4 → TS4 → S5). The second formate, which so far has stayed hydrogen bonded to the asparagines 78 and 311 without participating in the reaction, now loses its hydrogen to Cys79 to become a formyl

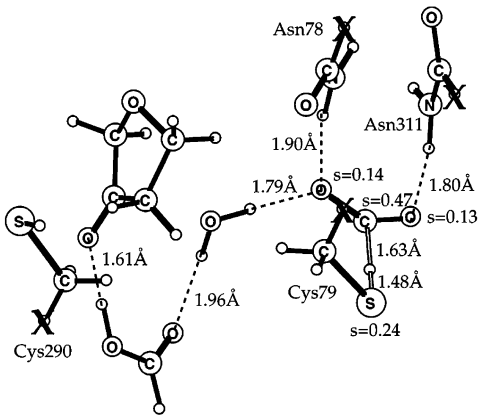

Figure 7. Transition state (TS4) for the fourth step.

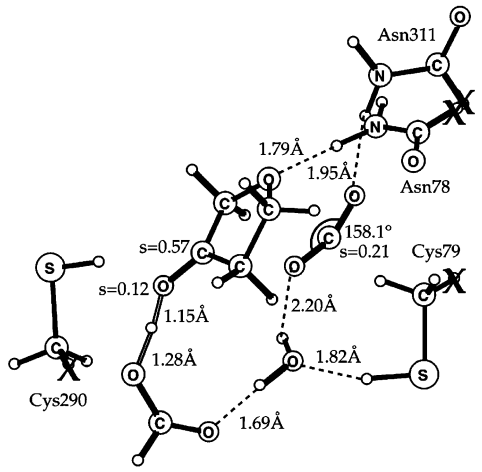

Figure 8. Transition state (TS5) for the fifth step.

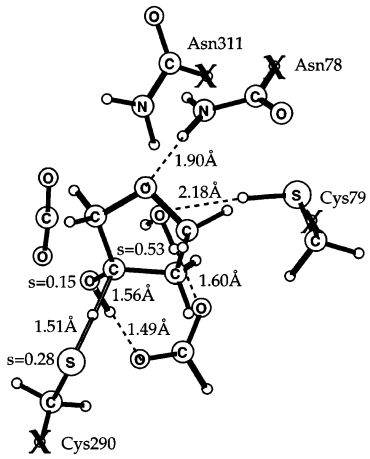

Figure 9. Transition state (TS6) for the sixth step.

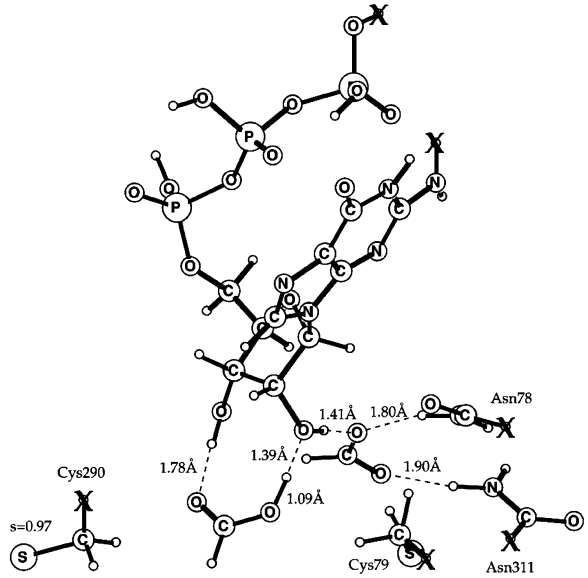

Figure 10. Starting structure S1 for the large model.

radical anion. Initially, the formate hydrogen is quite a long distance away from Cys79 (6.3 Å), but the rearrangements take place at a relatively low energetic cost (TS at −2.7 kcal/mol, Figure 7). At this point, basis set effects are substantial and remain so for the rest of the reaction. The explanation is that the double-ζ basis set is not sufficient for calculating the energies of either the formyl radical or the carbon dioxide.

The proposed roles of the asparagines can be studied by examining the energy needed to create a formyl radical without them. Some experimental results suggest that they are needed to hold the formyl radical in place. Mutational studies[33] show that some enzymatic activity is retained when one of the asparagines is replaced with alanine, whereas a double mutant resulted in a complete loss of activity. Calculations (6-311G-(d,p)) on small models with only a SCH_3-radical and $HCOO^-$ show that the product (formyl radical) is not even in a local minimum and therefore goes back to the reactant (cystein radical) unless the product is stabilized. This could occur, for instance, by a hydrogen bond to one of the formyl radical oxygens. Such a product was found, and the energy was 9.2 kcal/mol higher than the reactant (including zero-point and thermal energies). The same model, with an asparagine added, lowered the product to 5.3 kcal/mol (fixed atoms mimicking protein strain included). The same difficulty in obtaining a stable product was observed here as well. The last model, with two asparagines added, had a product with an energy of 4.3 kcal/mol. The corresponding value for the model in this study is 2.2 kcal/mol (Table 1). Although the transition state energies for any of these three models are not likely to exceed the rate-limiting step by themselves, the product is an intermediate during the rate-limiting step. Because of the above calculated product energy values, the rate-limiting barrier is predicted to be increased somewhat in the asparagine mutants, which should result in lower activity. The problem with stabilizing the product may also be a factor here, making it difficult, if not impossible, to obtain the products in the mutants.

Step 5: Electron Transfer and CO_2 Formation (S5 → TS5 → S6). The transition state in this step was the most difficult one to obtain in the entire reaction sequence, and it also turned out that this is the rate-limiting step for the present model. In order for the $(CO_2^{\bullet})^-$ to become CO_2, one electron has to be transferred to the 3′-site, a distance of approximately 5 Å. The most likely electron-transfer pathway goes over the other formate, which in turn has to lose its oxygen-bound hydrogen back to the substrate. The transition state is seen in Figure 8 where the formyl radical anion is straightening out to become a linear carbon dioxide at the same time as 3′O gets its proton back. To obtain the transition state, the O−C−O angle of the formyl radical anion turned out to be the key parameter. The rate-limiting barrier can now be calculated, which is the energy difference between this state (TS5, Table 1) and the lowest point in the reaction before this step (S4, Table 1). The rate-limiting barrier obtained is 11.7 kcal/mol (TS5 5.7 kcal/mol above S1). This is well below the experimentally determined limit of approximately 17 kcal/mol.

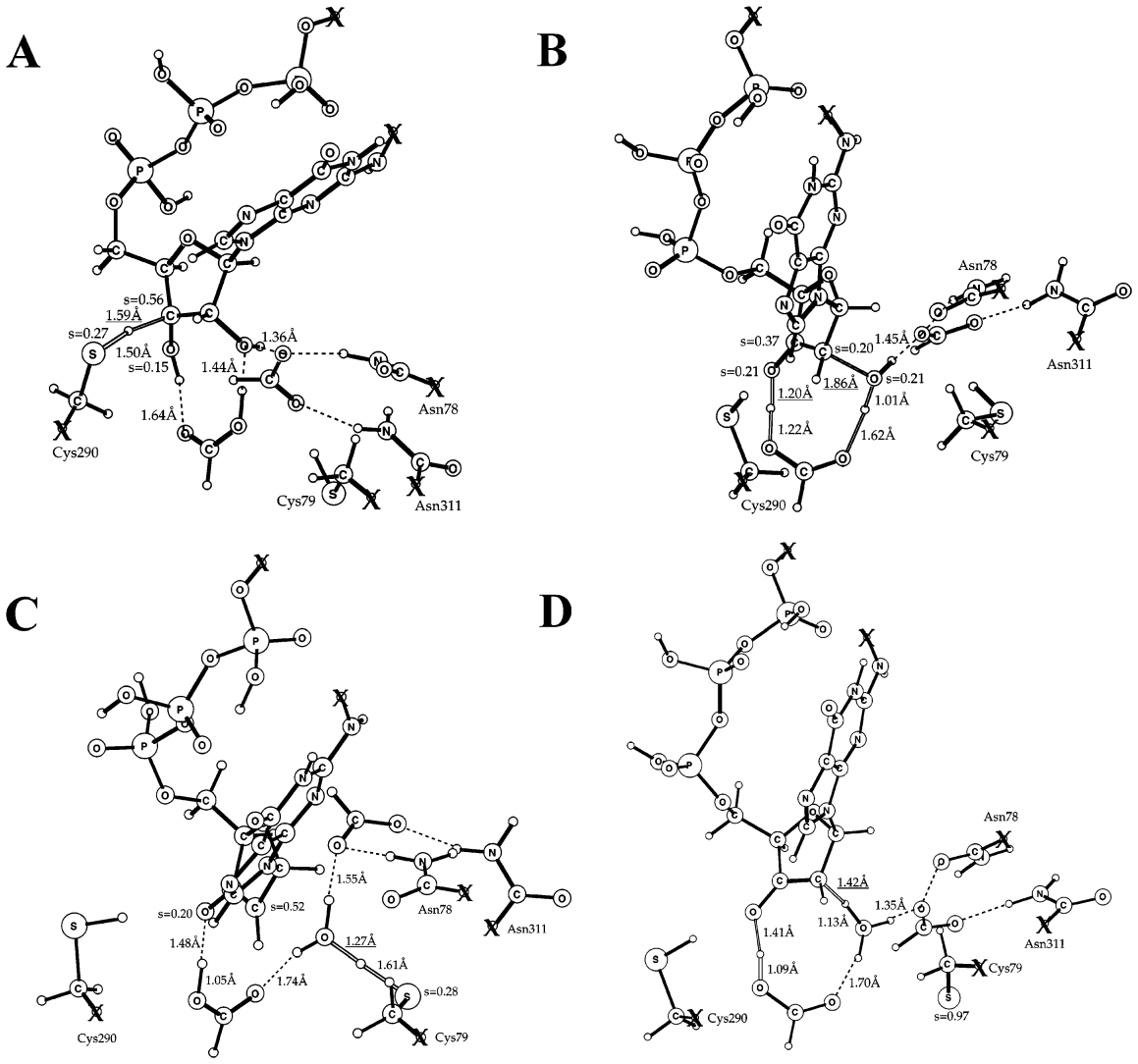

Figure 11. Large model transition states: (A) TS1; (B) TS2; (C) TS3a; (D) TS3b. The coordinates and distances that were frozen during geometry optimizations are indicated with an X and underlining.

It is interesting to compare this step with the corresponding step in class I RNR. In our parallel study,[26] it was found that the rate-limiting step occurs when the disulfur bond is formed. This bond is formed at the same time as an electron transfer occurs from the disulfur moiety to the 3′-side of the active site, a distance of approximately 8 Å. In addition, the formate also acts as a proton donor to 3′O of the substrate. A similar technical difficulty in locating this electron-transfer transition state was experienced there as well.

Step 6: The Returning of the 3′C Hydrogen (S6 → TS6 → S7). In this step, the hydrogen at Cys290 is returned to 3′C. At the small basis set level, this occurs over a barrier of 2.1 kcal/mol (Figure 9), but the barrier disappears when solvent and zero-point effects are added. This particular step is calculated to be endergonic by 1.5 kcal/mol, again because of solvent and zero-point effects. This step is in essence a reversal of step 1 as can be seen by the similar spin distribution and bond lengths of 3′H at the transition state, but the different energy profile implies that the surrounding structure (in particular near 2′) is of importance.

There are experiments confirming that Cys290 returns the hydrogen atom to 3′C at the end of the reaction. Labeling experiments on both class I RNR[48] and class III RNR[51] show that most of the 3′H is returned to 3′C, and only a small fraction ends up in water. This is consistent with the picture that the proton, while being attached to the cysteine during turnover, could be involved in proton exchange with the solution, but the substrate reduction rate is fast enough to let most of the protons return to 3′C without being exchanged.

Large Model Calculations. In the larger model, the triphosphate chain and guanine are added. Several problems were encountered for this model and the description below should be regarded as a progress report. Even though the endpoints were held fixed, the triphosphate chain turned out to be flexible enough to create several possible S1 conformations. These include some states with the phosphate chain hydrogen bonding to the base or the ribose ring, thereby lowering the energy of the state by several kcal/mol compared to conformations without such hydrogen bonds. This is especially troublesome considering that S1 is the state that all the other state energies are compared to. Differences in the orientation of the Cys290 radical also contribute to the energy differences between possible S1 configurations. After several attempts, a configuration was chosen which kept the structure as close to the small model as possible (Figure 10). In the following steps, the same phosphate chain folding was kept (without freezing any additional coordinates), avoiding formation of additional hydrogen bonds.

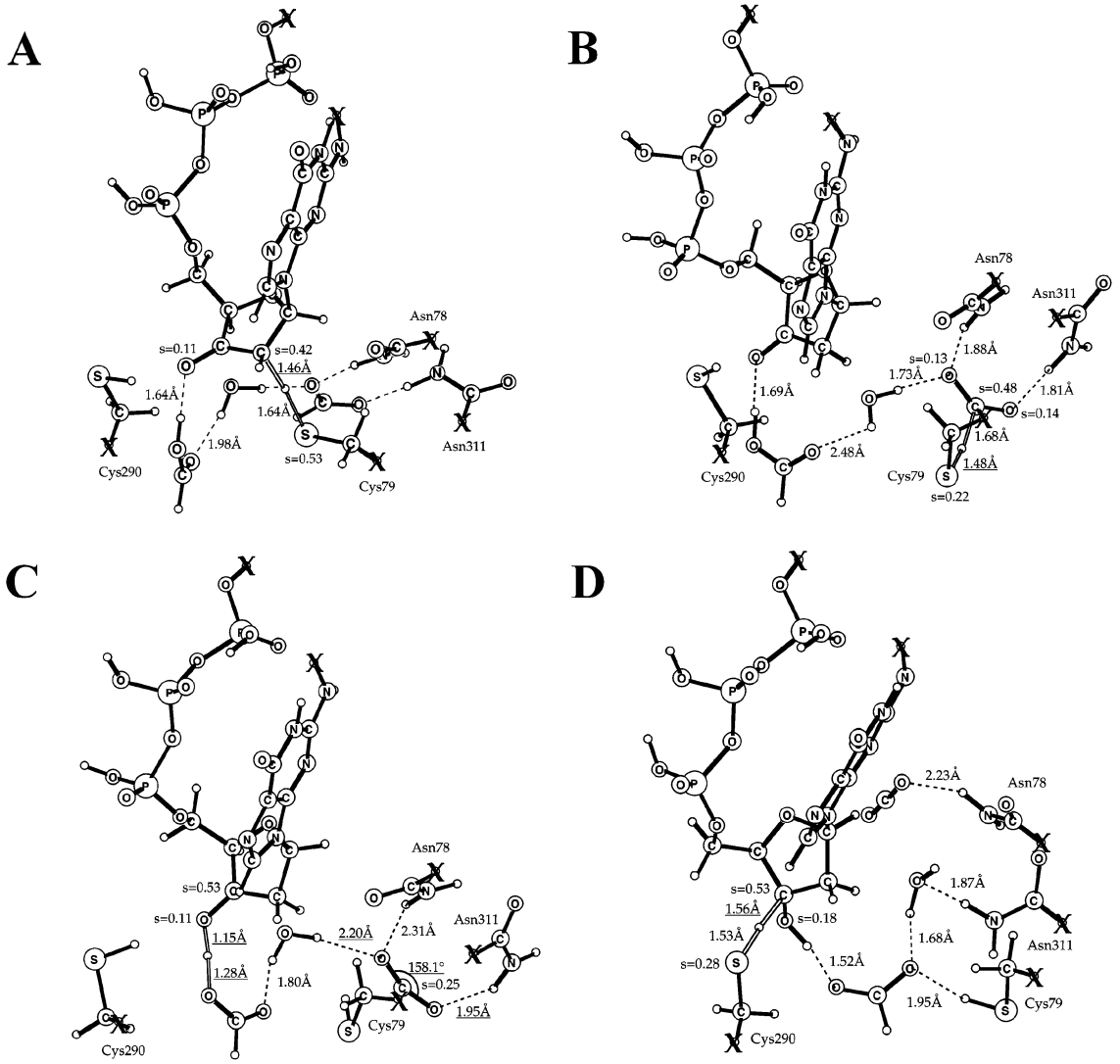

Figure 12. Large model transition states: (A) TS3; (B) TS4; (C) TS5; (D) TS6. The coordinates and frozen distances and angles during geometry optimizations are indicated with an X and underlining.

The barrier for the first step is calculated to be 11.0 kcal/mol (Figure 11A), with the product at 3.7 kcal/mol. The folding of the phosphate backbone chain is found to have some influence on how high the barrier can be, in combination with the direction that the ring-member oxygen points (in or out of the ring plane).

The large difference for the barrier between the two models was initially confusing, as earlier comparisons have shown that the energetic effects of enlarging models were minor.[53] Furthermore, the same deviation appeared in steps 3 and 6 (see below). In search of an explanation for this, the overlap picture between the TS1 structures of the small and large models was studied. It showed that the substrate ring was about 2 Å off of the position that was obtained for the substrate in the small model, possibly caused by the fixation of the rigid guanine base. This might cause greater strain for Cys290 to reach 3′C, with a higher barrier as a consequence. For the rest of the steps (except steps 3 and 6), there are only indirect interactions between the residues and the substrate ring through a functional group, which reduces the effects of the arbitrary fixation of the substrate. In a test run, the substrate (including the fixed atoms) was moved to a position that would correspond more exactly to the one in the small model. This gave a barrier of 10.3 kcal/mol. Although there was some gain in energy when the geometry changed, the solvent effects largely canceled this gain. Still, although the geometry strain may not be the only reason for the energy deviations, it seems likely that it contributes to it. It is also worth pointing out that even though this barrier is high, it is still lower than the rate-limiting barrier at step 5.

To model the concerted transition state of step 2 with the larger model, two key distances had to be frozen during the optimizations, as indicated in Figure 11B. The following steps 3a and 3b (Figure 11C,D) were without surprises. The geometries as well as the energetics were like those in the small model. However, the large structure calculations of TS3 (Figure 12A) gave a barrier of 15.1 kcal/mol, deviating strongly from the smaller model. Again, the somewhat artificial strain in the large model mentioned above could contribute to this deviation, as the same geometrical displacement has appeared here as in step 1 (i.e., a larger distance between Cys79 and the substrate than in the small model).

TS4 (Figure 12B) was readily obtained and found not to differ significantly from the small model, whereas TS5 (Figure 12C) turned out to be as difficult to obtain as it was in the small model. It required in the end the freezing of four bond lengths and one angle (the O−C−O angle of the formyl radical ion). The rate-limiting barrier is calculated to be 12.8 kcal/mol (9.9 compared to S1). The true value is however likely to be slightly lower when the distance and angle constraints are released. The

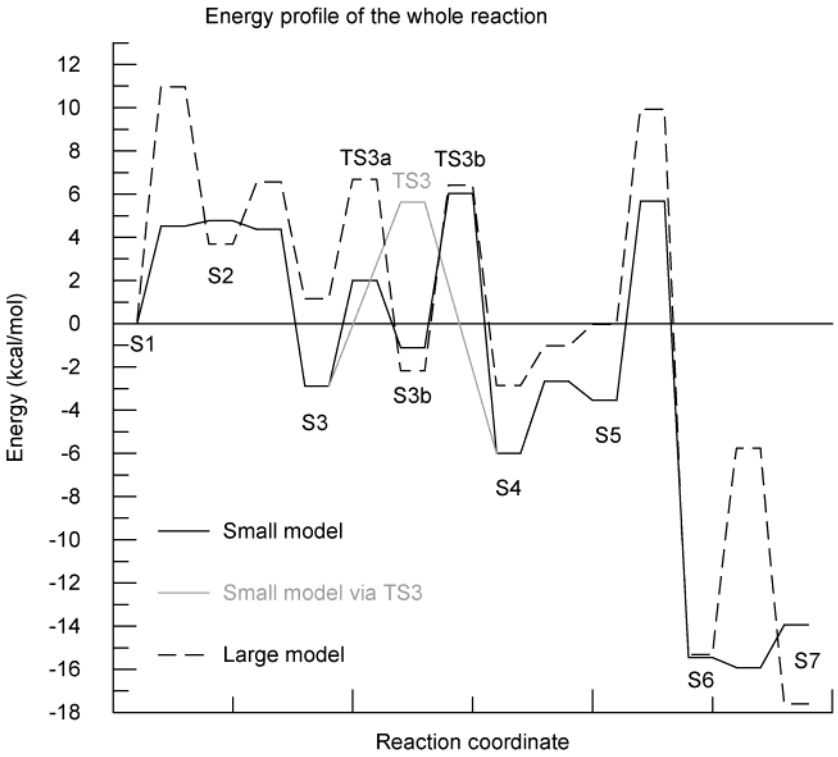

Figure 13. Energy profile of the substrate reaction.

solvent effects between the two models are quite different, lowering the barrier by 6.3 kcal/mol in the large model (as opposed to raising the barrier by 1.7 kcal/mol in the small model). Step 6 (Figure 12D) showed the same energy difference compared to the small model as was found in TS1 and TS3. Differences in geometry as well as CO_2 location in addition to large differential solvation effects could also contribute to this difference.

Summarizing the results of the large model, it is concluded that these are less reliable than those of the small model at the moment. To obtain more reliable results, a quantum mechanical/molecular mechanical (QM/MM) study is required. Such a study is at the research front, and no such study has yet appeared in the literature for a radical enzyme like the present one.

Conclusions

The entire reaction mechanism of class III ribonucleotide reductase is outlined in Scheme 3 and the whole reaction energy profile is shown in Figure 13. At the present stage the results of the small model are considered to be more reliable, and the following summary therefore refers to the small model. The main difference from previous modeling[38] is that two formates have been used rather than one. These two formates carry the proton necessary for the catalytic turnover, leading to a model with an overall charge of −1, compared to the previous neutral model. This should be more consistent with the fact that formate normally has a pK_a of 4, which should make it deprotonated in a neutral pH 7 solution. Following the suggestion that Asn78 and Asn311 could form a carboxylate binding site,[5,33] a negatively charged formate was put in a position to directly interact with the asparagines. The rate-limiting barrier for the present model is 11.7 kcal/mol, compared to 19.9 kcal/mol for the previous model. Given the improved results in terms of a lower rate-limiting barrier and compatibility with experiments (see below), the importance of this interaction is evident, although the explicit interaction remains to be experimentally verified.

In Scheme 3, there is a stoichiometric formation of dNTP and carbon dioxide, as well as the reduction of formate to carbon dioxide. If tritium-labeled $^3HCOO^-$ were to be used, the tritium would at first go to Cys79 over TS4 to S5, where it could exchange with water. As already pointed out in the previous study,[38] the water−cysteine proton exchange rate should be much faster than the *overall* enzymatic turnover rate (Scheme 3, S5 to S3 *including* the transition S7 to S1), which is only 3 s^{-1}. Experimental results suggest that the water−amino acid side chain proton exchange rate lies in the 100−15 000 s^{-1} range.[54] Protons at Cys79 would thus exchange with water at a rate at least 30 times the enzymatic turnover rate (probably much more depending on the actual cysteine−water proton exchange rate). This makes it almost certain that any proton derived from the formate ends up in the solution and that the new 2′H proton comes from the solvent. This is all verified by proton-labeling experimental results.[34,51]

Eliasson et al.[51] also found that the 3′H exchanged with the solvent as well, but to a very low degree (1−2%). This suggests that 3′H would first be abstracted by Cys290, where it could be the subject of a proton exchange process with water. However, in most cases 3′H is abstracted back by the substrate before this occurs. One can then make a crude estimate of the substrate turnover rate (Scheme 3, S1 to S7 *excluding* the transition S7 to S1) based on these numbers. Assuming the same water−cysteine proton exchange rate as above, the 1−2% exchange implies that the substrate reduction rate should correspond to the 5000−1 500 000 s^{-1} range, or 9.0−12.4 kcal/mol. Our computed barrier of 11.7 kcal/mol falls within this range.

The experimentally determined rate-limiting barrier of 17 kcal/mol is significantly higher than the value of 11.7 kcal/mol obtained here. Computed rate-limiting barriers that are substantially lower than the experimentally determined ones are very unusual in these types of studies. This indicates that the actual rate-limiting step for the enzymatic turnover probably lies

outside of the substrate reaction mechanism studied here. This conclusion is supported by the water−cysteine proton exchange discussion above. One possibility is that the rate-limiting step occurs during the transfer of the radical character to and from Cys290. Other possible rate-limiting steps are the substrate dNTP−NTP exchange after each turnover, or structural changes due to allosteric regulation. However, no further experimental information on this issue is yet available.

The neighboring asparagines facilitate the formyl radical anion formation from formate, a process that is likely to be energetically costly without the asparagines. Another conserved residue that could play a role in this process is Ser286. Overlaying the calculated structures on the crystal structure, Ser286 is seen to be positioned close to the substrate ring and the two asparagines, indicating that it may be important, for instance, in holding the formate close to the asparagines.

There have been suggestions in the literature that Cys79 is the hydrogen donor to 2′OH to form water.[39] Indeed, in the parallel study on class I RNR, this is precisely what is found.[26] In the present study, however, an optimized starting structure with a two-formate complex with 2′OH located in between was found, optimally positioned for step 2. The proton donor to 2′OH is then formic acid for the formation of water. If the water is to be formed with a proton from Cys79, the formic acid must (1) be in a less favorable position to donate its proton than the cysteine, (2) be in a position to donate its proton or electron or both at a later stage to either 2′C or Cys79, and (3) at all times avoid creating an energetically costly biradical. The last condition implies that when Cys79 gives its proton away to form water and the radical is retained on the substrate, Cys79 must become an anion. Although this is possible, no starting structure satisfying the first and second condition has been found.

In conclusion, it is not yet possible with quantum mechanical calculations at the presently attainable level of accuracy to prove reaction mechanisms for large biochemical systems. However, theoretical studies of a complex reaction like the present one show possible pathways and give a comprehensive picture of a detailed mechanism in agreement with experimental observations.

Supporting Information Available: Two XYZ files (small and large model) with *xyz*-coordinates for all stationary points with 10 linearly interpolated (not optimized) coordinates between each stationary point. This enables one to see the whole reaction mechanism as a "movie" with the appropriate software. This material is available free of charge via the Internet at http://pubs.acs.org.

References and Notes

(1) Reichard, P. *Science* **1993**, *260*, 1773.
(2) Sjöberg, B.-M. *Struct. Bonding* **1997**, *88*, 139.
(3) Stubbe, J.; van der Donk, W. A. *Chem. Rev.* **1998**, *98*, 705.
(4) Jordan, A.; Reichard, P. *Annu. Rev. Biochem.* **1998**, *67*, 71.
(5) Logan, D. T.; Andersson, J.; Sjöberg, B.-M.; Nordlund, P. *Science* **1999**, *283*, 1499.
(6) Uhlin, U.; Eklund, H. *Nature* **1994**, *370*, 533.
(7) Bollinger, J. M., Jr.; Tong, W. H.; Ravi, N.; Huynh, B. H.; Edmonson, D. E.; Stubbe, J. *J. Am. Chem. Soc.* **1994**, *116*, 8015.
(8) Davydov, A.; Liu, A.; Gräslund, A. *J. Inorg. Biochem.* **2000**, *80*, 213.
(9) Davydov, R. M.; Davydov, A.; Ingemarson, R.; Thelander, L.; Ehrenberg, A.; Gräslund, A. *Biochemistry* **1997**, *36*, 9093.
(10) Ochiai, E.; Mann, G. J.; Gräslund, A.; Thelander, L. *J. Biol. Chem.* **1990**, *265*, 15758.
(11) Riggs-Gelasco, P. J.; Shu, L.; Chen, S.; Burdi, D.; Huynh, B. H.; Que, L., Jr.; Stubbe, J. *J. Am. Chem. Soc.* **1998**, *120*, 849.
(12) Schmidt, P. P.; Rova, U.; Katterle, B.; Thelander, L.; Gräslund, A. *J. Biol. Chem.* **1998**, *273*, 21463.
(13) Sturgeon, B. E.; Burdi, D.; Chen, S.; Huynh, B.-H.; Edmondson, D. E.; Stubbe, J.; Hoffman, B. M. *J. Am. Chem. Soc.* **1996**, *118*, 7551.
(14) Himo, F.; Siegbahn, P. E. M. *J. Phys. Chem. B* **2000**, *104*, 7502.
(15) Mao, S. S.; Holler, T. P.; Yu, G. X.; Bollinger, J. M.; Booker, S.; Johnston, M. I.; Stubbe, J. *Biochemistry* **1992**, *31*, 9733.
(16) Siegbahn, P. E. M. *J. Am. Chem. Soc.* **1998**, *120*, 8417.
(17) Siegbahn, P. E. M.; Blomberg, M. R. A.; Crabtree, R. H. *Theor. Chem. Acc.* **1997**, *97*, 289.
(18) Siegbahn, P. E. M.; Eriksson, L.; Himo, F.; Pavlov, M. *J. Phys. Chem. B* **1998**, *102*, 10622.
(19) Stubbe, J. *Adv. Enzymol. Relat. Areas Mol. Biol.* **1990**, *63*, 349.
(20) Zipse, H. *Chem.—Eur. J.* **1999**, *5*, 3046.
(21) Åberg, A.; Hahne, S.; Karlsson, M.; Larsson, A.; Ormö, M.; Åhgren, A.; Sjöberg, B.-M. *J. Biol. Chem.* **1989**, *264*, 12249.
(22) Mao, S. S.; Yu, G. X.; Chalfoun, D.; Stubbe, J. *Biochemistry* **1992**, *31*, 9752.
(23) Lawrence, C. C.; Bennati, M.; Obias H. V.; Bar, G.; Griffin, R. G.; Stubbe, J. *Proc. Natl. Acad. Sci. U.S.A.* **1999**, *96*, 8979.
(24) Reichard, P. *Arch. Biochem. Biophys.* **2002**, *397*, 149.
(25) Sahlin, M.; Sjöberg, B.-M. *Subcell. Biochem.* **2000**, *35*, 405.
(26) Pelmenschikov, V.; Cho, K.-B.; Siegbahn, P. *J. Comput. Chem.* **2004**, *25*, 311.
(27) Liu, A.; Gräslund, A. *J. Biol. Chem.* **2000**, *275*, 12367.
(28) Ollagnier, S.; Mulliez, E.; Schmidt, P. P.; Eliasson, R.; Gaillard, J.; Deronzier, C.; Bergman, T.; Gräslund, A.; Reichard, P.; Fontecave, M. *J. Biol. Chem.* **1997**, *272*, 24216.
(29) Tamarit, J.; Gerez, C.; Meier, C.; Mulliez, E.; Trautwein, A.; Fontecave, M. *J. Biol. Chem.* **2000**, *275*, 15669.
(30) Young, P.; Andersson, J.; Sahlin, M.; Sjöberg, B.-M. *J. Biol. Chem.* **1996**, *271*, 20770.
(31) Olcott, M. C.; Andersson, J.; Sjöberg, B.-M. *J. Biol. Chem.* **1998**, *273*, 24853.
(32) Andersson, J.; Westman, M.; Sahlin, M.; Sjöberg, B.-M. *J. Biol. Chem.* **2000**, *275*, 19449.
(33) Andersson, J.; Bodevin, S.; Westman, M.; Sahlin, M.; Sjöberg, B.-M. *J. Biol. Chem.* **2001**, *276*, 40457.
(34) Mulliez, E.; Ollagnier, S.; Fontecave, M.; Eliasson, R.; Reichard, P. *Proc. Natl. Acad. Sci. U.S.A.* **1995**, *92*, 8759.
(35) Kozarich, J. W.; Brush, E. J. In *The enzymes*; Sigman, D. S. Ed; Academic Press: San Diego, CA, 1992; p 317.
(36) Wong, K. K.; Kozarich, J. W. In *Metal Ions in Biological Systems*; Sigel, H., Sigel, A. Eds; Marcel Dekker: New York, 1994; Vol. 30, p 279.
(37) Knappe, J.; Sawers, G. *FEMS Microbiol. Rev.* **1990**, *75*, 383.
(38) Cho, K.-B.; Himo, F.; Gräslund, A.; Siegbahn, P. E. M. *J. Phys. Chem. B* **2001**, *105*, 6445.
(39) Eklund, H.; Fontecave, M. *Structure* **1999**, *7*, R257.
(40) Eriksson, M.; Uhlin, U.; Ramaswamy, S.; Ekberg, M.; Regnström, K.; Sjöberg, B.-M.; Eklund, H. *Structure* **1997**, *5*, 1077.
(41) Kohn, W.; Sham, L. J. *Phys. Rev.* **1965**, *140*, A1133.
(42) Becke, A. D. *Phys. Rev. A* **1988**, *38*, 3098.
(43) Becke, A. D. *J. Chem. Phys.* **1993**, *98*, 1372.
(44) Becke, A. D. *J. Chem. Phys.* **1993**, *98*, 5648.
(45) *Jaguar*, version 4.2; Schrodinger, Inc.: Portland, OR, 2000.
(46) Frisch, M. J.; Trucks, G. W.; Schlegel, H. B.; Scuseria, G. E.; Robb, M. A.; Cheeseman, J. R.; Zakrzewski, V. G.; Montgomery, J. A., Jr.; Stratmann, R. E.; Burant, J. C.; Dapprich, S.; Millam, J. M.; Daniels, A. D.; Kudin, K. N.; Strain, M. C.; Farkas, O.; Tomasi, J.; Barone, V.; Cossi, M.; Cammi, R.; Mennucci, B.; Pomelli, C.; Adamo, C.; Clifford, S.; Ochterski, J.; Petersson, G. A.; Ayala, P. Y.; Cui, Q.; Morokuma, K.; Malick, D. K.; Rabuck, A. D.; Raghavachari, K.; Foresman, J. B.; Cioslowski, J.; Ortiz, J. V.; Stefanov, B. B.; Liu, G.; Liashenko, A.; Piskorz, P.; Komaromi, I.; Gomperts, R.; Martin, R. L.; Fox, D. J.; Keith, T.; Al-Laham, M. A.; Peng, C. Y.; Nanayakkara, A.; Gonzalez, C.; Challacombe, M.; Gill, P. M. W.; Johnson, B. G.; Chen, W.; Wong, M. W.; Andres, J. L.; Head-Gordon, M.; Replogle, E. S.; Pople, J. A. *Gaussian 98*, revision A.3/A.7; Gaussian, Inc.: Pittsburgh, PA, 1998.
(47) Gerfen, G. J.; van der Donk, W. A.; Yu, G.; McCarthy, J. R.; Jarvi, E. T.; Matthews, D. P.; Farrar, C.; Griffin, R. G.; Stubbe, J. *J. Am. Chem. Soc.* **1998**, *120*, 3823.
(48) Stubbe, J.; Ator, M.; Krenitsky, T. *J. Biol. Chem.* **1983**, *258*, 1625.
(49) van der Donk, W. A.; Gerfen, G. J.; Stubbe, J. *J. Am. Chem. Soc.* **1998**, *120*, 4252.
(50) Eliasson, R.; Pontis, E.; Eckstein, F.; Reichard, P. *J. Biol. Chem.* **1994**, *269*, 26116.
(51) Eliasson, R.; Reichard, P.; Mulliez, E.; Ollagnier, S.; Fontecave, M.; Liepinsh, E.; Otting, G. *Biochem. Biophys. Res. Commun.* **1995**, *214*, 28.
(52) Fernandes, P. A.; Eriksson, L. A.; Ramos, M. J. *Theor. Chem. Acc.* **2002**, *108*, 352.
(53) Pelmenschikov, V.; Blomberg, M. R. A.; Siegbahn, P. E. M. *JBIC, J. Biol. Inorg. Chem.* **2002**, *7*, 284.
(54) Liepinsh, E.; Otting, G. *Magn. Reson. Med.* **1996**, *35*, 30.